A Survey of Genuinely Multidimensional Upwinding echniques[1]

M.E.Hubbard

Numerical Analysis Report 7/93

Department of Mathematics
P.O.Box 220
University of Reading
Whiteknights
Reading
RG6 2AX
United Kingdom

[1]The work reported here forms part of the research programme of the Oxford/Reading Institute for Computational Fluid Dynamics and was supported by DRA Farnborough.

In the past few years upwind methods have become very popular in the modelling of advection dominated flows and in particular those which contain strong discontinuities. For more than a decade, these techniques have been used successfully to solve numerically the one-dimensional uler equations.

Unfortunately, the extension to higher dimensions is, as always, fraught with problems and has achieved only limited success until recently. Initial attempts were all based on the available one-dimensional methods and modelled the flow by solving simple Riemann problems across cell interfaces. This introduced an undesirable reliance on the computational mesh and such techniques were unable to adequately resolve shocks or shears which were not aligned with the grid. It was soon realised that it was necessary to incorporate genuinely multidimensional

2) The identification of the relevant propagation properties and directions within each cell, some form of pattern recognition, which depends on the system of equations under consideration. This requires the development of a wave decomposition model which splits the fluctuation into components each of which corresponds to a simple wave solution of the uler equations. The fluctuation due to each scalar wave can then be distributed using an advection scheme from step 1). Three types of decomposition, each due to a different author, are described in this report. Roe, [24, 25] and later [29], developed a number of wave models based on simple waves, while Rudgyard [18, 19] has recently developed his own simple wave models which, although similar, have different origins. Deconinck, Hirsch and Peuteman [10] devised an alternative strategy for decomposing the fluctuation. It is based on an attempt to diagonalise the system of uler equations and results in a set of maximally decoupled equations. Further details of these wave models may be found in [8, 19].

No single paper gives a detailed description of all the aspects of multidimensional upwinding, although Van Leer [16] and Roe and Deconinck [27, 9] give a good overview of all the techniques used above. A more thorough description of all the methods can be found by sampling notes from the VKI Lecture Series [12, 32, 8, 19]. All of these papers are concerned with the solution of the linear advection equation or, by extension, the uler equations, but Tomaich and Roe [7] show that the two-dimensional advection/diffusion equation can be solved in a similar way and suggest that a similar route may be used to create solvers for the full compressible Navier-Stokes equations.

The next section of this report covers fluctuation distribution schemes and their derivation. A description is given of a number of linear and nonlinear schemes and a brief comparison is presented highlighting the advantages and disadvantages of each of the most important schemes. Section 3 contains a description of the wave decomposition models due to Roe, Rudgyard and Deconinck/Hirsch and results from the first two of these are presented. Also described is a conservative linearisation of the two-dimensional uler equations, essential for these methods to be conservative, and a short comment is given on the implementation of the wave models. Section 4 describes one possible avenue for future work

2 Advection Schemes in Two Dimensions

Before attempting to model the full two-dimensional Euler equations it is necessary to consider the numerical solution of the linear advection equation

$$\frac{\partial u}{\partial t} + \vec{a} \cdot \vec{\nabla} u = 0, \tag{2.1}$$

where $\vec{a} \in \Re^2$ is a constant vector. This is to be solved numerically over an arbitrary triangulation of the region Ω, with appropriate conditions being imposed on the boundary of the domain, $\partial\Omega$.

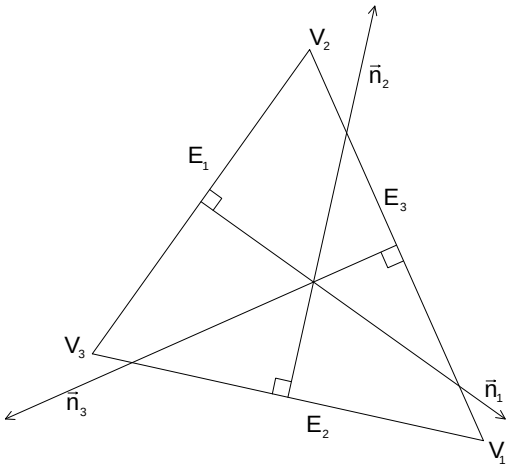

Figure 2.1: A general grid triangle with edges E_i, vertices V_i and normals $\vec{n}_i$.

The solution is represented as piecewise linear over a typical triangle T, such as that in figure 2.1, and can therefore be written as

$$u(x, y, t) = \sum_i u_i(t) w_i(x, y), \tag{2.2}$$

where $w_i(x, y)$ is the 'tent function' used in the application of linear finite elements and $u_i(t)$ can be considered as either the amplitude of w_i or the point value of u at $x = x_i, y = y_i$. Now, the integral of $\frac{\partial u}{\partial t}$ over an element T gives the fluctuation,

$$\phi_T = \int\int_{S_T} \frac{\partial u}{\partial t}\, dx\, dy = -\int\int_{S_T} \vec{a} \cdot \vec{\nabla} u\, dx\, dy = \oint_{\partial T} u\, \vec{a} \cdot d\vec{n}, \tag{2.3}$$

where ∂T is the boundary and S_T the area of T, and $d\vec{n}$ is the inward normal to the boundary of the element. Note that the fluctuation is related to the cell residual R_T through $\phi_T = -S_T R_T$, where S_T is the cell area, so the two can be easily interchanged in the theory presented below. Now, u varies linearly within each triangle, and hence along each side, so the fluctuation can be easily evaluated:

$$\begin{aligned} \phi_T &= \frac{1}{2}(u_1 + u_2)\, \vec{a} \cdot \vec{n}_3 + \frac{1}{2}(u_2 + u_3)\, \vec{a} \cdot \vec{n}_1 + \frac{1}{2}(u_3 + u_1)\, \vec{a} \cdot \vec{n}_2 \\ &= -\frac{1}{2} u_1\, \vec{a} \cdot \vec{n}_1 - \frac{1}{2} u_2\, \vec{a} \cdot \vec{n}_2 - \frac{1}{2} u_3\, \vec{a} \cdot \vec{n}_3, \end{aligned} \tag{2.4}$$

where is the normal to edge scaled by the length of edge . Thus, the fluctuation can be expressed simply as

$$= \tag{2 5}$$

where

$$= \frac{1}{2} \tag{2 6}$$

The are important because they can be used to determine the direction of flow through an edge: if 0 then flow enters the triangle through edge but if 0, edge is an outflow edge. It is also useful to note that, since

$$+ \quad + \quad = 0 \tag{2 7}$$

we can write

$$= 0 \tag{2 8}$$

which leads to a number of alternative formulae for which will be used later.

Now, integrating the first term of equation (2.1) over the whole domain using the expression (2.2) gives

$$\text{—} \quad = \quad \frac{1}{3} \quad \text{——} + \text{——} + \text{——} \quad = \quad \text{——} \tag{2 9}$$

where is the area of the median dual cell around node , one third the total area of the triangles having as a vertex. By using a simple backward time differencing this leads naturally to a fluctuation distribution scheme where, for each triangle of the domain in turn, three replacements are carried out:

$$+ \quad \Delta \tag{2 10}$$

The are simply weights which determine the distribution of the fluctuation to the nodes of the triangle. It can easily be shown that this gives a conservative

which for a given triangle can be written

$$\begin{aligned} S_1 u_1^{n+1} &= S_1 u_1^n - \alpha_1^T \Delta t(k_1 u_1^n + k_2 u_2^n + k_3 u_3^n) + TFOT \\ S_2 u_2^{n+1} &= S_2 u_2^n - \alpha_2^T \Delta t(k_1 u_1^n + k_2 u_2^n + k_3 u_3^n) + TFOT \\ S_3 u_3^{n+1} &= S_3 u_3^n - \alpha_3^T \Delta t(k_1 u_1^n + k_2 u_2^n + k_3 u_3^n) + TFOT, \end{aligned} \tag{2.13}$$

where TFOT stands for 'terms from other triangles'.

It is the 'fluctuation distribution' form (2.13) that will be considered from now on, and not the nodal form (2.12), since it can be used to treat each cell individually and, with the above restriction, the activity within a cell only affects the nodes at its own vertices.

A basis has now been created for the design of advection schemes on linear triangles, but it is now necessary to decide how the fluctuation within each triangle should be distributed to its vertices. In doing this, it is necessary to take a number of factors into consideration. It has already been shown that conservation is easily guaranteed and that a compact stencil is ensured for the schemes considered. Two further desirable properties are those of positivity and of linearity preservation, defined below.

Positivity means that every value at the new time level, u_i^{n+1}, can be written as a convex combination of old values. So for a linear scheme, written

$$u_i^{n+1} = \sum_k c_k u_k^n, \tag{2.14}$$

where the coefficients c_k are independent of the data u_i^n, positivity requires all the c_k to be positive or zero for each node. Consistency is given by

$$\sum_k c_k = 1. \tag{2.15}$$

This guarantees a maximum principle for the discrete steady state solution, thus prohibiting the occurrence of new extrema and imposing stability on the explicit scheme [32]. A stronger but more easily verifiable condition is local positivity which requires that the contribution of each triangle separately is positive.

Linearity preservation requires that the scheme preserves the exact steady state solution whenever this is a linear function in space for an arbitrary triangulation of the domain. This is closely related to the idea of second order accuracy of finite difference schemes, although it is an accuracy requirement on the space discretisation only. This property can be verified using the fact that a scheme of the form (2.13) is linearity preserving if and only if, for any triangle T, the coefficients α_i^T are bounded as ϕ_T tends to zero [32].

It should be noted that, when written in the form (2.13), the only possibilities of having a linear scheme are for the coefficients α_i^T to be independent of the

data, in which case the scheme is linearity preserving, or for

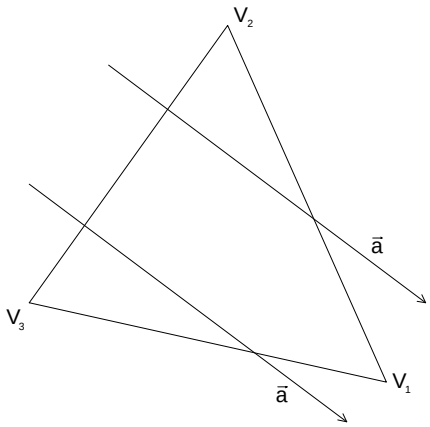

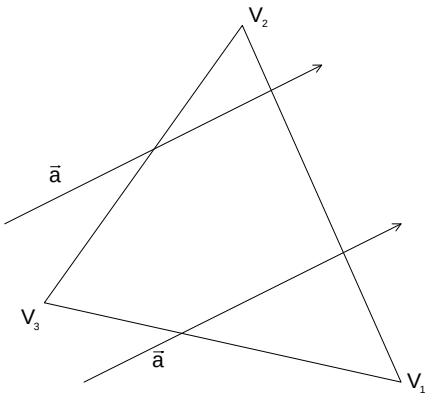

allowable time step and the most narrow stencil (hence its name, the N(arrow) scheme). A similar optimal scheme has also been derived for use on quadrilateral and hexahedral grids [28].

As explained above, if a triangle within the domain has only one inflow side then the whole fluctuation can be sent to the downstream node, which is the optimal choice. Now, for triangles with two inflow sides, specifying that the scheme is positive means that it cannot be linearity preserving, so the coefficients in equation (2.13) can be expressed as

$$= — \tag{2 18}$$

where the are linear functions of the data summing to . Now suppose that the inflow sides are and , 0. The upwind philosophy suggests that nothing is sent to the upstream vertex , so

$$= 0 \qquad + \quad = \tag{2 19}$$

Now, making use of (2.8) the fluctuation may be written

$$= \quad (\quad) \quad (\quad) \tag{2 20}$$

so the most general two target scheme with linear functions for is,

$$\begin{aligned} = \quad & \Delta \ (\ (\quad) + \ (\quad) \quad (\quad)) + \\ = \quad & \Delta \ (\ (\quad) \quad (\quad) + \ (\quad)) + \end{aligned} \tag{2.21}$$

where and are arbitrary parameters, independent of the data and is unchanged. Now, local positivity of the scheme requires the following quantities to be non-negative:

$$\begin{aligned} & 1 \quad \frac{\Delta}{—}(\quad + \quad) \qquad + \\ & 1 \quad \frac{\Delta}{—}(\quad + \quad) \qquad + \end{aligned} \tag{2.22}$$

For small enough Δ) this is tr)(u8L84Hsanthe)(

The restriction placed on the time step by requiring global positivity is obtained by taking into account the coefficients of u_j for all triangles T meeting at node j and gives

$$\Delta t \leq \frac{S_j}{{}_T \max(0, k_j^T)}. \tag{2.25}$$

This is also the linear scheme with the most narrow stencil, since setting p_1 and p_2 to zero eliminates the contribution from the outermost points of the stencil, figure 2.3a.

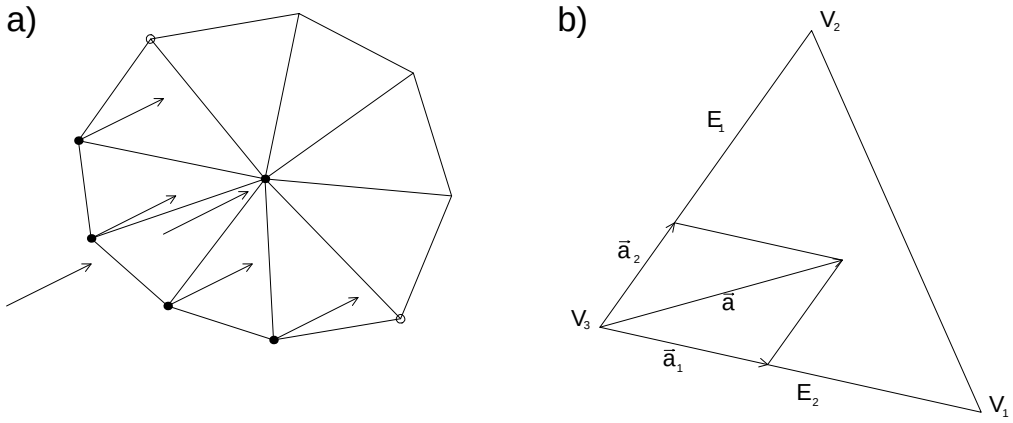

Figure 2.3: The stencil of the N-scheme (left) and the graphical interpretation of the two inflow side case (right).

The effect of this scheme can be easily visualised, figure 2.3b, by considering $\vec{a}$ as the sum of components parallel to E_1 and E_2,

$$\vec{a} = \vec{a}_1 + \vec{a}_2. \tag{2.26}$$

Now, the fluctuation due to $\vec{a}_1$ is sent to V_1 since only E_2 is an inflow side for it, and the fluctuation due to $\vec{a}_2$ is sent to V_2.

The next class of linear schemes to be considered are those satisfying linearity preservation. The upwind schemes of this form given here are known as low diffusion schemes due to the relatively small amount of numerical diffusion obtained in comparison with the linear positive upwind schemes.

As before, the single target strategy is used for all triangles with only one inflow side, but for the two inflow side case the general equations (2.13) are considered with the coefficients α independent of the data. Two simple strategies can now be found which are both based on dividing the triangle along the velocity vector, as in figure 2.4.

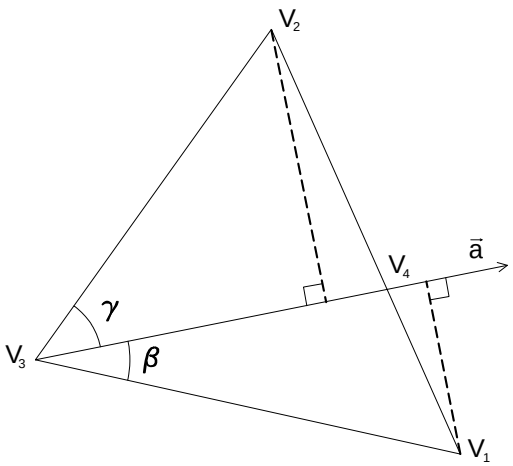

Figure 2.4: The graphical interpretation of the two low diffusion schemes.

The first low diffusion scheme (LDA) is obtained by taking the area of the dividing triangles as the criterion. Referring to figure 2.4, that part of the fluctuation evaluated over sub-triangle 314 is used to update and the part evaluated over 234 to update . The resulting coefficients are thus given by

$$= \quad - \quad = \quad \frac{342}{123} \quad = \quad \frac{42}{12342}$$

$$= \qquad \qquad \qquad =$$

$$- \qquad \frac{\qquad}{\qquad} \qquad \frac{\qquad}{\qquad}$$

$$\frac{\qquad}{\qquad} \qquad \frac{\qquad}{\qquad}$$

$$\frac{\qquad}{\qquad} \qquad \frac{\qquad}{\qquad}$$

a hybrid approach to modelling. Here, different schemes are used in different regions of the flow and it is convenient that all the schemes can be written in a fluctuation distribution form so that the method is consistent throughout the domain.

Two well known central schemes can be easily represented as fluctuation distribution schemes. A Lax-Wendroff type scheme is obtained by defining the coefficients in equation (2.13) to be

$$\alpha = \frac{1}{3} + \frac{1}{2}\frac{k\,\Delta t}{S}. \tag{2.30}$$

This can be shown to be equivalent to a mass-lumped Taylor-Galerkin finite element method on linear triangles. The choice

$$\alpha = \frac{1}{3}, \tag{2.31}$$

obtained by dropping the dissipative contribution in the above scheme is identical with Jameson's [2] central finite volume scheme for unstructured triangular meshes, although it lacks the Runge-Kutta time stepping required to impose stability. It is also equivalent to a mass-lumped Galerkin finite element method on linear triangles. Both of these methods satisfy the linearity preservation property but not positivity.

Alternative upwind schemes may also be represented in this way, including a mass-lumped streamline upwind Petrov-Galerkin (SUPG) finite element method, which gives a linearity preserving scheme, and a first order positive upwind finite volume scheme.

A number of linear schemes have now been described and although all of them are consistent and conservative, none is both positive and linearity preserving. In order to have both these properties, nonlinear schemes must be considered, schemes of the form (2.14) where the coefficients depend on the data.

The nonlinear schemes presented here make use of the fact that when considering events within a triangle , the advection velocity $\vec{a}$ can be replaced in the analysis by any vector of the form

$$\vec{a} = \vec{a} + \lambda\vec{a}\ , \tag{2.32}$$

where $\vec{a}$ is orthogonal to the local value of $\vec{u}$ and λ is an arbitrary parameter. This is because the addition of this component has no effect on the fluctuation within the cell:

$$(\vec{a} + \lambda\vec{a}\ )\quad \vec{u} = \vec{a} \qquad + \qquad = \tag{2 33}$$

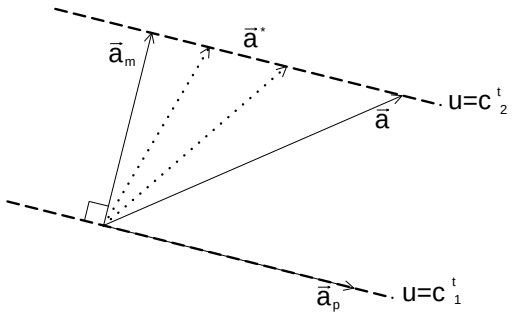

Figure 2.5: The gradient dependent advection velocity.

In particular, the gradient dependent advection velocity, shown in figure 2.5, can be used,

$$= (\qquad) \tag{2 34}$$

where

$$= \text{——} = \begin{matrix} \cos \\ \sin \end{matrix} \tag{2 35}$$

is the unit vector in the direction, , of the local gradient of the solution and perpendicular to the level lines of the solution.

Now, since is assumed to have linear variation in space (so is constant), the solution of the two-dimensional linear advection problem (2.1) evolves in time according to

$$\begin{aligned} (\quad) &= \quad (\qquad) + \qquad (\Delta \qquad \Delta \ ) \\ &= \quad (\qquad) + \qquad (\qquad\qquad \Delta \ ) \end{aligned} \tag{2.36}$$

where represents the initial conditions. These two equivalent forms of the solution to (2.1) show that using the gradient dependent advection velocity still corresponds to the plane wave solution of the linear advection equation, and that using the intrinsically two-dimensional quantity corresponds to the notion that waves propagate normal to their level lines.

An important effect of using as the advection speed is that, as steady state is approached, becomes very small, and so the form of the stability bounds of the N-scheme, (2.25), implies that much larger time steps can be taken as steady state is approached. This is possible because the time scale relevant to stability is that on which a level line of the solution migrates across a cell, not the time taken by a particle moving with velocity [32].

As a consequence of (2.33) any linear combination of and can be con-

There are two main NN schemes (where NN stands for nonlinear and narrow) which have been developed, both of which use the gradient dependent advection velocity to produce a scheme which is both positive and linearity preserving and, since they are based on the N-scheme described earlier, have a narrow stencil.

The first of these, developed at the VKI, uses the N scheme (2.24), but with the based on the gradient dependent advection velocity, so

$$= \frac{1}{2} \qquad = \frac{1}{2}(\qquad)(\qquad) \tag{2 37}$$

where is the unit vector in the direction of and is the scaled inward normal to edge . Now, since

$$= \qquad\qquad = \tag{2 38}$$

where = is the edge vector from vertex to vertex of the triangle, then assuming that the inflow sides are and , figure 2.1, substitution of these values of into equations (2.24) gives

$$\begin{aligned} &= \qquad + \Delta \quad \frac{(\qquad)(\qquad)}{2} + \\ &= \qquad + \Delta \quad \frac{(\qquad)(\qquad)}{2} + \end{aligned} \tag{2.39}$$

where the fluctuation has been introduced, is the area of the triangle under consideration and is the area of the median dual cell around node . This leads to weights used in the distribution of the fluctuation which are

$$= \frac{(\qquad)(\qquad)}{2} \qquad = \frac{\qquad\qquad}{\qquad\qquad}$$

a)

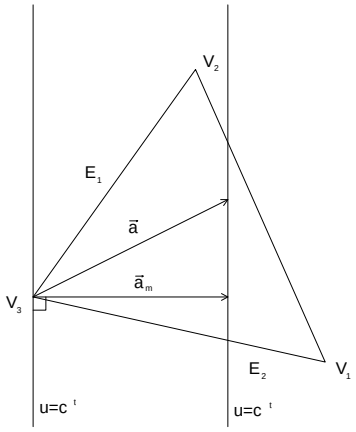

b)

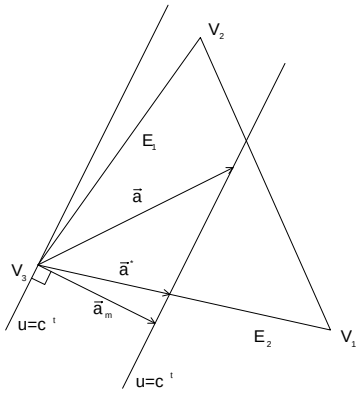

original coefficients k , given by

$$\begin{aligned} k &= k + \lambda(u \quad u) \\ k &= k + \lambda(u \quad u) \\ k &= k + \lambda(u \quad u), \end{aligned} \tag{2.42}$$

which can be chosen to maximise the allowable time step. In [32], it is shown that this is achieved by considering the N scheme (2.24) with the values for the k given above and then choosing λ to give the largest possible time step, of the form (2.25). The optimal scheme derived in this way can be interpreted by considering level lines of the solution. If the level line through the downstream vertex passes through the triangle then the optimal time step is obtained by sending the whole fluctuation to one vertex, which depends on the sign of the fluctuation. Otherwise, a two target scheme is used which keeps the direction of $\vec{u}$ fixed during the update. If the two inflow sides due to the simple advection velocity are E and E , then this leads to the coefficients

$$\alpha = \frac{S\,(u \quad u)}{(\quad) + (\quad)} \qquad = \frac{(\quad)}{(\quad) + (\quad)} \tag{2 43}$$

when converted to the form (2.13). This leads to the algorithm:

a) If a triangle has only one inflow side according to the original advection velocity , then send the whole fluctuation to the downstream node.

b) If the triangle has two inflow sides, say and , according to , then consider the scheme:

   i) If the level line of the solution at the upstream node of the triangle doesn't pass through the triangle, ( )( ) 0, then update both downstream vertices using (2.43).

   ii) If the level line of the solution at does pass through the triangle, send the whole fluctuation to one node, if ( ) 0, otherwise.

Rudgyard [19] has also devised a positive, linearity preserving scheme which is a variant of Roe's level scheme and has been designed to depend on all aspects of the data in a continuous way in an attempt to improve robustness. The derivation is based on the fact that, if the fluctuation within a cell is negative and has its minimum value within the cell at node , then a locally positive scheme will not reduce this value any further. Similarly, for 0 the scheme will not increase the maximum nodal value. This leads to a restriction on the time step

ensures that the resulting scheme is positive. Such a method may still update nodes on the upstream side of the cell, affecting convergence, but the distribution coefficients can be chosen to avoid this and to give linearity preservation by remaining bounded as ϕ_T tends to zero:

$$\begin{aligned} \alpha_i &= \frac{(k_i^+)^2(u_i - u_k)}{(k_i^+)^2(u_i - u_k) + (k_j^+)^2(u_j - u_k)} \\ \alpha_j &= \frac{(k_j^+)^2(u_j - u_k)}{(k_i^+)^2(u_i - u_k) + (k_j^+)^2(u_j - u_k)} \\ \alpha_k &= 0, \end{aligned} \tag{2.44}$$

where

$$k_i^+ = \frac{1}{2}(1 + sign(k_i))|k_i| \tag{2.45}$$

and node k is chosen so that

$$\begin{aligned} u_k &= \min(u_1, u_2, u_3) \quad if \quad \phi_T < 0 \\ u_k &= \max(u_1, u_2, u_3) \quad if \quad \phi_T > 0. \end{aligned} \tag{2.46}$$

The scheme is easily modified to deal with cases when two or more vertices of the triangle have the same value.

As with linear schemes, a number of common nonlinear schemes can be expressed in the form of a fluctuation distribution scheme. In [32], the nonlinear gradient dependent advection velocity has been used to create a scheme of this form equivalent to a mass-lumped SUPG scheme with a shock capturing term.

2.6 Results

In the literature there are two main test cases, introduced by Speckreijse [34], which appear frequently when these schemes are being studied in two dimensions. A small selection of results is presented here simply to highlight some of the most important points.

The first test case consists of linear advection with constant velocity $\vec{a} = (\cos\frac{\pi}{8}, \sin\frac{\pi}{8})$ throughout the unit square $[0,1] \times [0,1]$ with boundary conditions $u = 0$ at the lower boundary and $u = 1$ at the left boundary. This problem models a contact or shear discontinuity.

Three different types of grid have been used to produce the results in this report. All of them have been constructed from a cartesian grid. The triangular grids, shown in figure 2.7, have then been produced by inserting diagonals between the bottom left and top right vertices of each square (Grid A), the bottom right and top left vertices (Grid C) and by alternating between the two (Grid B).

Figures 2.8-2.11 show the results of this test case on a grid of type A based on a 33×33 cartesian mesh, using four different schemes, the N scheme, the VKI NN

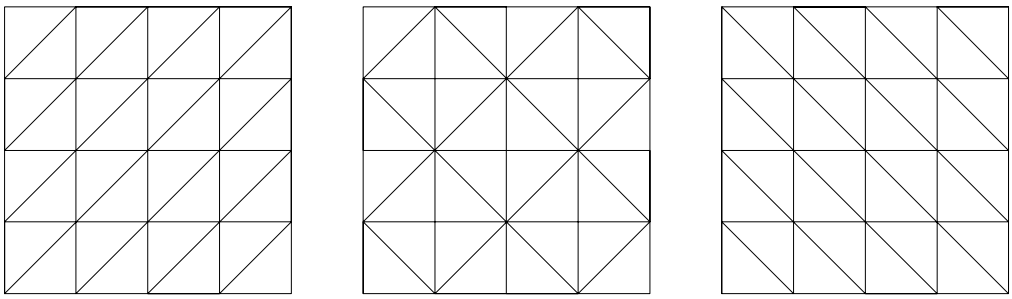

Figure 2.7: The three types of grid used for the results.

scheme, the LDA scheme, and the Lax-Wendroff scheme. The second of these has been chosen as representative of all the nonlinear schemes presented here since they all give very similar results [32]. In each case, the initial conditions used were $u = 1$ on the left boundary, $x = 0$, and $u = 0$ elsewhere and all four schemes gave steady state solutions which converged to machine accuracy.

As expected, the two non-positive schemes, LDA and Lax-Wendroff, give oscillations in the solution close to the discontinuity, with those produced by the Lax-Wendroff scheme being much larger. (The LDB scheme gives much the same results as the LDA scheme.) However, since they satisfy linearity preservation, they also give the sharpest discontinuities, closely followed by the NN scheme which is also linearity preserving. The two positive schemes, N and NN, both give solutions with no oscillations at the discontinuity. The NN scheme gives the sharper definition of the two, although in all cases the shear continues to become more diffuse across the domain. It appears from this that the NN scheme is the best shown here, having both higher order accuracy (experiments have shown it to be roughly of order 1.6) and giving a monotone solution across the discontinuity. As yet, though, it is not clear which of these nonlinear narrow schemes shows the most promise, particularly in its application to the uler equations.

What this doesn't show is the grid dependence of these algorithms. This is demonstrated in figures 2.12-2.15 which show results from both this case and a second shear test case which differs only in the advection velocity, $\vec{a} = (\cos\frac{\pi}{4}, \sin\frac{\pi}{4})$. Both cases were run on 33×33 grids of types A and C. As can be seen, when the diagonals of the grid are exactly parallel with the advection velocity, the discontinuity is captured extremely well across just one line of cells, but this deteriorates rapidly as the diagonals becomes less aligned with the flow, until the worst case is reached when the diagonals are orthogonal to the flow. In practice grids are unlikely to emulate either of the two extremes, but will produce something closer to the intermediate solutions, figures 2.13 and 2.14. In fact, for a grid of type B, figure 2.9 shows the worst possible grid alignment.

This observation can be considered in two ways. The pessimistic view would be that any grid dependence is undesirable since it leads to much uncertainty over the results, particularly when matters are complicated by considering systems of nonlinear equations. Alternatively, the best result obtained above, figure 2.12, is extremely good, so it may be advantageous to develop a grid adaption algorithm which will align edges of grid cells with the direction of the flow, resulting in very sharp discontinuities. Again, complications will arise when this is extended to the uler equations, but the potential benefits are huge.

The second of the test cases of Speckreijse consists of clockwise circular advec-

type B. ven with the NN scheme, after one revolution the peak of the cone has been reduced to only 18.5% of its original value and it has been heavily diffused, figure 2.22. Fortunately, this is not a problem for steady state calculations but improvements to the time accuracy of these schemes will need to be made to these schemes before time varying flows can be modelled with any confidence using these methods.

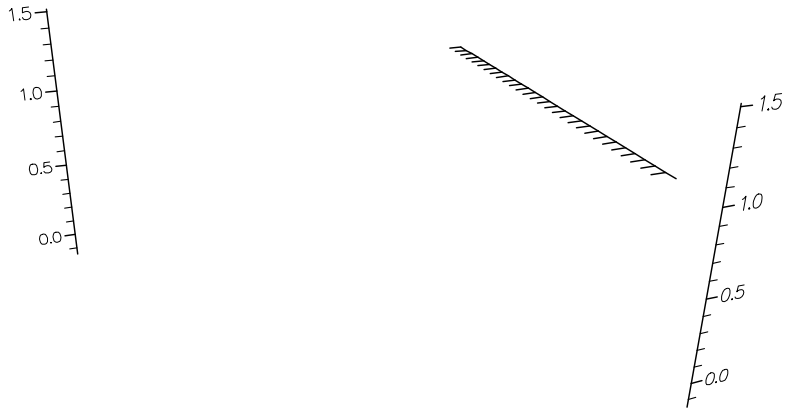
1.5
1.0
0.5
0.0
1.5
1.0
0.5
0.0

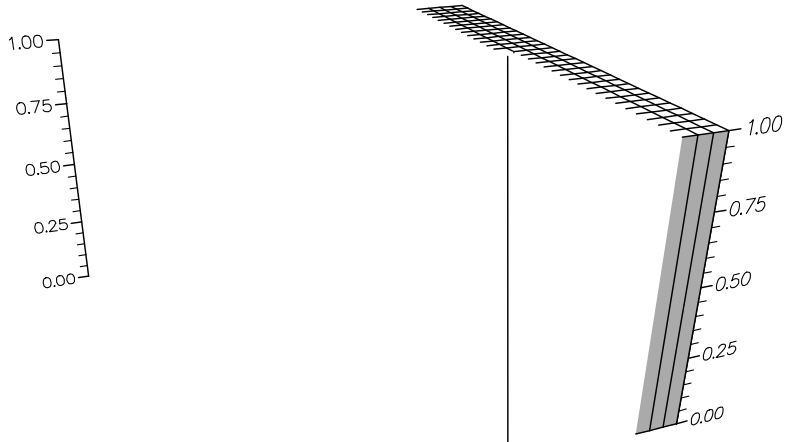
1.00
0.75
0.50
0.25
0.00
1.00
0.75
0.50
0.25
0.00

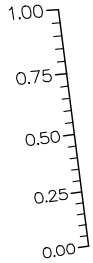
1.00
0.75
0.50
0.25
0.00

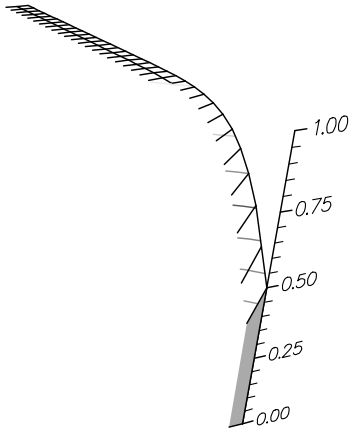
1.00
0.75
0.50
0.25
0.00

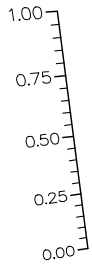
1.00
0.75
0.50
0.25
0.00


0.25
0.00

3 Extension to the Euler Equations

The schemes presented in the previous section have all been developed to solve the linear advection equation in two dimensions, but they can also be considered as an integral part of the solution of systems of nonlinear conservation laws such as the uler equations,

$$\frac{\partial}{\partial} + \frac{\partial}{\partial} + \frac{\partial}{\partial} = \_ \tag{3 1}$$

where

$$\_ = \qquad \_ = \qquad + \qquad \_ = \qquad + \tag{3 2}$$
$$(\ + \ ) \qquad (\ + \ )$$

in which is density, and are the - and -velocities, is pressure, and is total energy, related to the other variables by an equation of state which, for a perfect gas, is

$$= \frac{}{1} + \frac{1}{2} (\quad + \quad) \tag{3 3}$$

The uler equations in the form (3.1) cannot immediately be solved using the multidimensional upwinding techniques described in this paper. Instead, it is necessary to consider the quasilinear form

$$\frac{\partial}{\partial} + \frac{\partial}{\partial} + \frac{\partial}{\partial} = \_ \tag{3 4}$$

where $= \frac{\partial}{\partial}$ and $= \frac{\partial}{\partial}$ are the local Jacobian matrices of the system. It is this system which must be discretised over the domain and then solved. In order to achieve this, consistent approximations to the Jacobians and are required within each cell, which can be calculated using the nodal values of the data.

In one dimension a conservative approximation to the Jacobian is obtained by requiring the approximate Jacobian to satisfy a property U [22]. In two dimensions the linearisation is forced to be conservative by constructing the local approximations to the Jacobians, ˜ and ˜, so that they satisfy the following two-dimensional version of property U:

The linearisation is consistent, in the sense that

$$\tilde{}(\_ \ \_ \ \_) = \quad (\_) \qquad \tilde{} \ \_ \ \_ \ \_ \qquad \_$$

$$\_ \ \_ \ \_ \qquad \_ \ \_ \ \_$$

The identities

$$\overline{\overline{\quad}}\,\tilde{\ }(\_\ \_\ \_)\overline{\overline{\quad}} \qquad \overline{\overline{\quad}}\,\tilde{\ }(\_\ \_\ \_)\overline{\overline{\quad}} \tag{3 6}$$

are satisfied for any $\_$, $\_$, $\_$.

The third of these criteria is critical since it ensures that the linearisation is conservative and is crucial for sharply capturing steady discontinuities. However, it requires that consistent averages, $\overline{\overline{\quad}}$, $\overline{\overline{\quad}}$, $\overline{\overline{\quad}}$ and $\overline{\overline{\quad}}$, be found for the gradients within each cell.

It could now be assumed that $\_$, the vector of conserved variables, varies linearly over each triangular cell, so $\_$ is constant within each cell. This unfor-

The problem which now arises is due to the fact that the Jacobian matrices A and B which arise from the uler equations in two dimensions do not share a common set of eigenvectors, and so the linearised system cannot be decoupled immediately into a set of simple advection equations. To overcome this, Roe [25] suggested expressing the fluctuation as a sum of simple wave solutions.

Consider the conservative linearisation of the uler equations in the primitive variables.

$$\frac{\partial \underline{\mathbf{q}}}{\partial t} + \tilde{A}\,\widehat{\frac{\partial \underline{\mathbf{q}}}{\partial x}} + \tilde{B}\,\widehat{\frac{\partial \underline{\mathbf{q}}}{\partial y}} = \underline{\mathbf{0}} \tag{3.21}$$

A simple wave solution of this system takes the form

$$\underline{\mathbf{q}} = \underline{\mathbf{q}}(\zeta), \qquad \zeta = \vec{x} \quad \vec{n} \qquad \lambda\ t, \tag{3.22}$$

where $\vec{n} \quad = (\cos\theta, \sin\theta)$ gives the direction of propagation and λ the speed of the wave. In fact

$$\vec{\underline{\mathbf{q}}} = \frac{d\underline{\mathbf{u}}}{d\zeta}\vec{n}\ , \tag{3.23}$$

and substituting these into (3.21) gives

$$\lambda\ \frac{d\underline{\mathbf{u}}}{d\zeta} + (\tilde{A}\ \cos\theta + \tilde{B}\ \sin\theta)\frac{d\underline{\mathbf{u}}}{d\zeta} = \underline{\mathbf{0}}. \tag{3.24}$$

Therefore, $=$ is a right eigenvector of the matrix $\tilde{A}\ \cos\theta + \tilde{B}\ \sin\theta$ and λ is the corresponding eigenvalue. Now for each direction θ there exist four distinct eigenvectors with corresponding eigenvalues, each of which corresponds to a different type of wave. In the primitive variables these correspond to an entropy wave,

$$\lambda = u\cos\theta + v\sin\theta, \qquad \underline{\mathbf{r}} = (1, 0, 0, 0) \quad , \tag{3.25}$$

a shear wave,

$$\lambda = u\cos\theta + v\sin\theta, \qquad \underline{\mathbf{r}} = \rho\,(0, \sin\theta, \quad \cos\theta, 0) \quad , \tag{3.26}$$

and two acoustic waves,

$$\lambda = u\cos\theta + v\sin\theta \quad c, \qquad \underline{\mathbf{r}} = \frac{1}{2} \quad \frac{\rho}{c}, \quad \cos\theta, \quad \sin\theta, \rho c) \quad . \tag{3.27}$$

A more complete description of the $\widehat{\text{derivation}}$ and effect of these simple waves can be found in [8, 3].

The eigenvectors of the uler equations in conserved variables can easily be obtained using the transformation

$$\underline{\mathbf{r}} \quad = \tilde{M}\ \underline{\mathbf{r}} \quad , \tag{3.28}$$

where $\tilde{}$ is the approximation to , (3.18). The eigenvalues remain unchanged.

Now, the assumption that the parameter vector variables vary linearly in space implies that their gradients are constant at a particular time level within each cell. Thus, consistent cell averaged values of the gradients of the primitive variables can be found using (3.20) and these can be expressed within each cell as the superposition of a number of discrete waves

$$\_ = \quad \bar{\_} \tag{3 29}$$

where $\bar{\_}$ is a cell averaged value of the eigenvector which has the corresponding eigenvalue $\bar{}$. This corresponds to a sum of waves of strength propagating in the direction of the unit vector with speed $\bar{}$.

Now from (3.19), the cell residual can be expressed as

$$\_ = \quad = = \tilde{} \quad \bar{} \; \bar{\_} = \quad \bar{} \; \bar{\_} \tag{3 30}$$

where $\bar{\_}$ are the eigenvectors corresponding to the conserved variables. Note that this implies that it is only the eigenvectors which are altered by a change of variables and that the wave speeds $\bar{}$ and wave strengths are independent of such changes.

It is also important to note that the velocities $\bar{}$ which are obtained for this

$\_$

$\_$

Roe [23, 25] was one of the first to propose a suitable wave decomposition, using simple wave theory as the basis for his model. He suggested that a finite number of 'active' waves should be selected to represent the flow and reduce the decomposition (3.29) to a limited number of terms. Although there are many such wave models that have the 8 free parameters to fit the 8 degrees of freedom, there are four that appear in the literature, chosen for their simplicity (they give simple real-valued expressions for all data) and their realistic representation of the flow.

ach of these models has four orthogonal waves representing acoustic disturbances, acoustic waves at angles , + –, + and + —, which provides five free parameters, the angle (taken to be in the range [– +–] as one of the four waves is bound to lie there) and four strengths , , and . All the models also have an entropy wave which uses an angle and a strength as two more free parameter78[ec]0970[0'7N[pF'fi079['flkk2F0902tif9[,]F09N7flfi07l7nd]F'9fi707l7ns]F'fi079

The other three wave models differ only in the choice of the sixth wave, so the only alterations to the above equations required are in the terms involving the strength k and the direction ζ.

This system can be easily solved for the unknown strengths and angles [23] to get them in terms of the gradients of the primitive variables. The resulting acoustic waves propagate in directions parallel to the principal strain rate axes of the local flow, as desired in the kinematic analysis, and the shear wave strength turns out to be the local vorticity within the cell. Solving for the direction and strength of the entropy wave gives precisely the direction and modulus of the entropy gradient.

ach of the waves now has a strength α^k, an eigenvalue (speed) $\overline{\lambda}^k$, an eigenvector $\underline{\overline{\mathbf{r}}}^k$ and a direction θ_k which can be substituted into (3.30) to produce the fluctuations due to each simple wave. These can then be distributed using one of the schemes described in the previous section.

3.4 Rudgyard's Wave Models

More recently Rudgyard [18, 19] has proposed an alternative wave decomposition which again uses simple waves but is derived by a slightly different approach. This can be considered as a mesh independent directional splitting technique which uses the fact (shown earlier) that for a particular direction θ there are four types of wave, corresponding to an entropy wave, a shear wave and two acoustic waves. It also makes use of the identity

$$\vec{\nabla}\,\underline{\mathbf{q}} \equiv \frac{-(\vec{s}_{\theta_2}\cdot\vec{\nabla}\,\underline{\mathbf{q}})\vec{n}_{\theta_1} + (\vec{s}_{\theta_1}\cdot\vec{\nabla}\,\underline{\mathbf{q}})\vec{n}_{\theta_2}}{\sin(\theta_2-\theta_1)}, \tag{3.33}$$

where $\vec{s}_\theta = (-\sin\theta, \cos\theta)$ is the unit vector orthogonal to $\vec{n}_\theta$. The wave model is obtained by projecting each term on the right hand side of (3.33) on to the eigenvectors corresponding to the angles θ_1 and θ_2 respectively, to give

$$\vec{\nabla}\,\underline{\mathbf{q}} = \sum_{k=1}^{4} \alpha_{\theta_1}^{(k)}\,\underline{\mathbf{r}}_{\theta_1}^{(k)}\,\vec{n}_{\theta_1} + \sum_{k=1}^{4} \alpha_{\theta_2}^{(k)}\,\underline{\mathbf{r}}_{\theta_2}^{(k)}\,\vec{n}_{\theta_2}, \tag{3.34}$$

where

$$\alpha_{\theta_1}^{(k)} = -\frac{\vec{s}_{\theta_2}\cdot(\underline{\mathbf{l}}_{\theta_1}^{(k)}\vec{\nabla}\,\underline{\mathbf{q}})}{\sin(\theta_2-\theta_1)}, \qquad \alpha_{\theta_2}^{(k)} = \frac{\vec{s}_{\theta_1}\cdot(\underline{\mathbf{l}}_{\theta_2}^{(k)}\vec{\nabla}\,\underline{\mathbf{q}})}{\sin(\theta_2-\theta_1)}. \tag{3.35}$$

These are the 8 wave strengths which are the free parameters for this model. The $\underline{\mathbf{l}}_{\theta_i}^{(k)}$ are the left eigenvectors of the matrix $\tilde{A}'\cos\theta + \tilde{B}'\sin\theta$ with corresponding right eigenvectors $\underline{\mathbf{r}}_{\theta_i}^{(k)}$.

A number of different wave models can be derived by choosing the definition of the angles θ_1 and θ_2. An obvious choice is $\theta_1 = 0$ and $\theta_2 = \frac{\pi}{2}$ for which the discrete x- and y-derivatives are treated independently. However, it is far more

beneficial to select the angles with a view to minimising the number of 'active' waves present in the decomposition by choosing directions which set either the strength or speed of particular waves to zero. This means that these waves do not contribute to the decomposition of the fluctuation and so reduces the computational effort. Alternatively, the angles can be chosen to align with physically important gradients to improve the shock capturing capabilities of the method [33].

Now, the eigenvectors for the entropy waves are independent of the direction, so the number of waves present in the model can be reduced by combining them to form one wave. It turns out that the single entropy wave produced has a strength and direction which are simply the modulus and direction of the entropy gradient, as was the case with each of Roe's models. The gradient decomposition can now be written

$$\_ = \quad \_ \quad + \quad \_ \quad + \quad \_ \tag{3 36}$$

A five wave model can be obtained by choosing

$$= \tan \quad \begin{matrix} — \\ — \\ — \end{matrix} \qquad = \tan \quad \frac{—— \quad ——}{—— + ——} \tag{3 37}$$

which sets the strengths of two of the acoustic waves, and , to zero. The resulting decomposition has an entropy wave, two acoustic waves and a shear wave based on the angle , and a single shear wave based on .

Alternatively, the angles can be chosen to set wave speeds to zero so that although the waves appear in the gradient decomposition, they make no contribution to the fluctuation. A 'streamwise' splitting involves setting _ and _ to be parallel and orthogonal to the streamlines, which makes the speed of one of the shear waves zero. The 'Mach angle' splitting sets the speed of two sound waves to zero by choosing

$$= \tan \quad \frac{+ \ (\qquad 1)^{-}}{(\qquad 1)^{-}} \qquad = \tan \quad \frac{(\qquad 1)^{-}}{+ \ (\qquad 1)^{-}} \tag{3 38}$$

an entropy wave. One of the shear waves is then chosen to be orthogonal to the streamlines, forcing its speed to be zero. Four wave models have a great appeal in the context of accuracy. When more waves are used, the fluctuation, a four-vector, is decomposed into more than four discrete waves and so a zero residual does not generally give zero wave strengths. In fact, a locally steady flow is represented as a state of equilibrium between the discrete waves [23] and, in the above models, only the entropy wave is guaranteed to have zero strength. This is contrary to the philosophy of the fluctuation distribution schemes of section 2, and of cell vertex methods in general, for which a zero fluctuation within a cell should imply a null contribution to its nodes. In particular it calls into question the usefulness of requiring a scalar distribution scheme to satisfy linearity preservation in order to improve its accuracy, when this could be largely negated by the wave model used. Rudgyard [19] describes in more detail how decompositions may be derived to overcome these problems and suggests that four wave models may represent the way forward.

3.5 The Deconinck/Hirsch Wave Model

A third separate approach to wave decomposition has been proposed by Deconinck, Hirsch and Peuteman [10]. Unlike the previous methods it does not consider simple waves, but is based on converting the uler equations to a set of maximally decoupled scalar advection equations by using characteristic theory. No results from this wave model are presented in this report but some may be found in [32] where it is studied in conjunction with a number of the distribution schemes presented in section 2.

The quasilinear system (3.4) can be transformed to a set of characteristic variables $\underline{\mathbf{W}}$ using the matrix $M_W = \frac{\partial \mathbf{u}}{\partial \underline{\mathbf{W}}}$, giving

$$\frac{\partial \underline{\mathbf{W}}}{\partial t} + M_W^{-1} A M_W \frac{\partial \underline{\mathbf{W}}}{\partial x} + M_W^{-1} B M_W \frac{\partial \underline{\mathbf{W}}}{\partial y} = \underline{\mathbf{0}}. \tag{3.39}$$

It is not possible to decouple the system by choosing M_W such that $M_W^{-1} A M_W$ and $M_W^{-1} B M_W$ are both diagonal since A and B do not commute. Instead M_W and $\underline{\mathbf{W}}$ are sought which satisfy

$$M_W^{-1} A M_W = \quad ^x + C^x, \qquad M_W^{-1} B M_W = \quad ^y + C^y, \tag{3.40}$$

with

$$C^x \frac{\partial \underline{\mathbf{W}}}{\partial x} + C^y \frac{\partial \underline{\mathbf{W}}}{\partial y} = \underline{\mathbf{0}}, \tag{3.41}$$

where ^{x} and ^{y} are diagonal matrices. The uler equations would then become

$$\frac{\partial \underline{\mathbf{W}}}{\partial t} + \quad ^x \frac{\partial \underline{\mathbf{W}}}{\partial x} + \quad ^y \frac{\partial \underline{\mathbf{W}}}{\partial y} = \underline{\mathbf{0}}, \tag{3.42}$$

a set of four decoupled equations.

In [8] it is shown how the uler equations can be written as an equivalent set of compatibility relations. These can be written as

$$\begin{aligned}
&\text{——} + \qquad = 0 \qquad = \quad \frac{1}{\text{—}} \\
&\text{——} + \qquad + \frac{1}{\text{—}} \qquad = 0 \qquad = \\
&\text{——} + (\quad + \quad) \quad + \quad (\quad) = 0 \qquad = \quad + \frac{1}{\text{—}} \\
&\text{——} + (\quad) \quad + \quad (\quad) = 0 \qquad = \quad + \frac{1}{\text{—}}
\end{aligned} \tag{3.43}$$

where the are unit vectors normal to , the direction of propagation of the wavefront in the x-y plane, and = ( ) is the velocity vector.

This set of compatibility relations can now be identified with the decoupled system (3.42) provided that the coupling terms in the last three equations can be made to vanish. This can be done by choosing a particular characteristic surface such that locally

$$= 0 \qquad (\quad) = 0 \qquad = \tag{3 44}$$

The first condition is easily satisfied and corresponds to a shear wave propagating in the direction of the local pressure gradient. The conditions on and are more complicated. The coupling term in the third and fourth equations can be written in terms of the local strain rate tensor, , giving

$$(\quad) = (\quad) = 0 \tag{3 45}$$

where

$$= \begin{matrix} \text{—} & \text{-} \ \text{—} + \text{—} \\ \text{-} \ \text{—} + \text{—} & \text{—} \end{matrix} \tag{3 46}$$

Now (3.45) has two real solutions for only if has eigenvalues, , , of different sign, and so a complete decoupling can be obtained by choosing to b one of these solutions.

Otherwise, the coupling term cannot be set to zero, so it is instead minimised

conditions of uniform flow at the freestream Mach number and then run until a steady state solution was reached. The flow tangency condition is applied at solid walls while freestream boundaries are treated using a combination extrapolation from the interior and Riemann invariant boundary conditions, depending on the speed and direction of the flow. In all cases local time stepping has been used with a CFL number of 0 8.

The first set of results uses a grid of type B and show Roe's wave model D used with the VKI NN scheme. Figure 3.3 shows a plot of Mach number contours for test case 1) and the same test case using the Lax-Wendroff scheme is shown in figure 3.4. Of the two, Lax-Wendroff is much the better since it does at least give contours which are symmetric about the centre of the bump. The upwind solution seems to 'lean in the wind', particularly near the lower wall, and the problem occurs whichever mesh is used. It may be associated with the solid wall boundary conditions, but is also exhibited by other wave models such as those of Rudgyard and Parpia [14], although the phenomenon is less noticeable in results presented by Roe [21] on a finer mesh.

Figure 3.5 shows the results from using Roe's model D on the second, transonic, test case. Again the plot is of Mach number contours and it shows a shock of about the right strength in the correct position on the bump. It is captured across one cell of the grid, although this isn't generally the case when the shock is not aligned with the grid. This test case has also been considered by Rudgyard [19], but of his methods only the four wave model produces a shock with the correct strength and position, and this unfortunately gives an expansion shock upstream of the desired one, a problem also exhibited by Parpia's five wave model.

Figure 3.6 shows Mach number contours for the third test case using Roe's model D again. ach of the two oblique shocks formed at the endRoea7'[r]F07N[endRo]F09ws are captured well, as are the reflected shocks at both the upper and lower surfaces of the channel. In fact the solution looks very good and, unlike in the scalar case, the shock does not spread out downstream, although the nonlinearity of the system does cause very small oscillations in the solution in front of the first shock which are visible here because of the contour at = 1 5.

The main problem with this model, and with all ea7'[897'[the]%t0'70'fl82fi2PtF7fi0902t[wave]F
creasey Converged
solutions ve een hieved ted 32, 4]
seems to be dependent on many things such as the problem itf and boundary conditions, so before these schemes becomey useful someetd must be devised robustness. een k'79

problem is the calculation of the wave directions, and that since they depend on the local flow gradients, which are piecewise constant, they are unable to settle down to a steady state value. Recent work has also been carried out on the non-linear advection schemes to improve their convergence properties when applied to a two-dimensional version of the inviscid Burgers' equation [17] and this may well improve results for the uler equations as well.

With Rudgyard's models this is not such a serious problem. Some of his wave models, such as his Mach angle splitting, do not use the gradients to calculate the angles, and all solutions presented here which use this model have been converged to machine accuracy. For his other models it is easy to freeze the directions within each cell to attain converged solutions. This, though, is clearly an undesirable method of achieving robustness when time varying flows are considered. Also, it is not obvious how to freeze or lag these angles for Roe's models since their calculation involves solving a set of 8 equations (3.31).

This gives Rudgyard's models a significant advantage over those of Roe and others. However, figure 3.8 shows that, for the third test case, his Mach angle splitting identifies each of the shocks which are supposed to be present, but does not give as sharp a definition as Roe's model D. Rudgyard's own results [19] indicate that this difference is not as great as is shown here but he does emphasise that this model is only valid for mainly supersonic flows. He also shows that these multidimensional methods compare favourably with a standard MUSCL TVD scheme. Both of these wave models though show a huge improvement over Rudgyard's dimensional splitting, figure 3.7, in which none of the shocks are adequately captured.

Figures 3.9 and 3.10, produced with Rudgyard's Mach angle splitting on grids of type A and C, show that the grid dependence seen in the linear advection schemes of the previous section is inherited by these methods, although since the fluctuation is now split into a number of separate waves, all with different directions, the problem is not as noticeable. It is still obvious though that discontinuities are captured much more sharply if they are aligned with the diagonals of the grid, *eg.* the shock formed at the front of the bump is captured more sharply by the type A grid, indicating that it may again be possible to use grid adaption to great effect. Roe's wave model is more susceptible to the vagaries of grid generation and the problem of robustness becomes even more apparent when an unfavourable grid is used. However, it also means that on a grid where the cell edges are aligned with the shocks Roe's wave model gives much sharper discontinuities than Rudgyard's model. This grid dependence should be solely due to the orientation of the flow relative to the mesh edges, and therefore only depend on the propagation directions of the simple waves, since the wave model itself is independent of the grid.

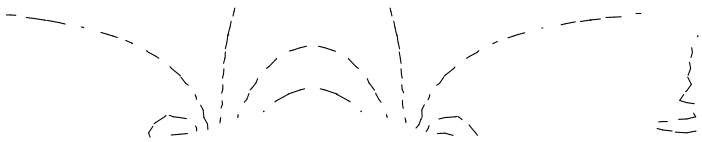

4 A Hybrid Approach

Many points have been highlighted by a large number of authors in the study of the methods described in this report. Probably the most important is that multidimensional upwinding schemes are still very much in the early stages of their development. However, even now there are indications as to the strengths and weaknesses of these methods.

At present it seems that, although these methods are good at modelling discontinuous flow features such as shocks and shears, they are inadequate for the smoother, purely subsonic flows. However, subsonic flow and smooth flow in general can be modelled very well by far less complicated schemes, such as the Lax-Wendroff type scheme described in section 2.3. This suggests that this scheme could be used throughout the smooth regions of the flow, while the more expensive multidimensional upwinding techniques are used only in the vicinity of flow features which the simple scheme is unable to cope with, thus considerably reducing the computational effort required. A brief study of the use of such a hybrid approach in one dimension has been conducted with considerable success [20].

Just one set of results is presented here, since this work has only just begun. In this case a monitor has been introduced to detect shocks which simply consists of checking the density gradient within each cell. During each time step all the cells with a density gradient over a specified value were flagged, as were all adjacent cells. Then, in every flagged cell, multidimensional upwinding was used (in this case Rudgyard's Mach angle splitting with the VKI NN-scheme), while the Lax-Wendroff scheme was used everywhere else. To increase the robustness of the method it was necessary to ensure that cells did not alternate between schemes every few time steps. This was achieved by first introducing a lag so that a cell, once flagged, retained the flag for at least the next 100 iterations and secondly, as the steady state was approached, a flagged cell became permanently flagged. The pictures shown are of results which have been converged to machine precision.

Figure 4.1 shows the Mach number contours, plotted at intervals of 0 05, for the hybrid scheme used on a 65 33 grid of type B, where multidimensional upwinding is used in cells where 2 and in adjacent triangles (these cells are superimposed in figure 4.2)F‘08p570[esults]F‘087N[whic]097 flesulTI[Mac]rase [Mac]reart 2,D.bJb.

methods were used. There, it was resolved by moving the interface between the regions where the two schemes were used further away from the shock. While this may well remove the wiggles parallel to the shocks, it will probably have little effect on the 'corner' wiggles which are intrinsically multidimensional phenomena.

One of the big advantages of using the hybrid scheme is its speed. A single Lax-Wendroff time step takes roughly one third the cpu time of a single time

5 onclusions

It is obvious from the results presented in this report and by other authors that these genuinely multidimensional methods are still in the early stages of their development. However, compact schemes have been developed for use on triangular and tetrahedral meshes which show much promise for the future.

Of the two main aspects of the work, the fluctuation distribution schemes are probably the better understood. Optimal linear positive and linearity preserving schemes have been developed, although it is necessary to consider nonlinear schemes before one can be both positive (monotone) and linearity preserving (second order). The so-called nonlinear narrow schemes are generally considered to be the best of those presented, although it is not clear which of the variants is the most promising.

Common to all of these schemes is a grid dependence. Discontinuities are captured far more shwhich more ono7H[e]8[on]0fifififi02nrhoug‘[n]F0987dfifififimore rgnh eonfoN[d-
the mesors

scheme is only used close to more 'interesting' parts of the flow. Initial results indicate that results can be obtained by this method which are of similar quality to those produced using multidimensional methods alone, but in less than 40% of the time.

Acknowledgements

M. . Hubbard is supported financially by a contract funded by DRA Farnborough. He wishes to thank Dr. M.J. Baines and Dr. A. Priestley, of the Mathematics Department, University of Reading, and Dr. M.A. Rudgyard, of C RFACS, Toulouse, for their advice and assistance during this work.

References

[1] A.Dadone and B.Grossman. A rotated upwind scheme for the uler equations. Paper 91-0635, AIAA, 1991.

[2] A.Jameson and D.Mavriplis. Finite volume solution of the two-dimensional uler equations on a regular triangular mesh. , 24:611–618, 1986.

[3] A.Majda. , volume 53 of . Springer-Verlag, 1984.

[4] C.L.Rumsey, B.van Leer, and P.L.Roe. A grid-independent approximate Riemann solver with applications to the uler and Navier-Stokes equations. Paper 91-1530, AIAA, 1991.

[5] D.W.Levy. . PhD thesis, University of Michigan, 1990.

[6] D.W.Levy, K.G.

[12] H.Deconinck, R.Struijs, and P.L.Roe. Fluctuation splitting for multidimensional convection problems: an alternative to finite volume and finite element

[25] P.L.Roe. Discrete models for the numerical analysis of time-dependent multidimensional gas dynamics. , 63:458–476, 1986.

[26] P.L.Roe. Optimum upwind advection on triangular meshes. Technical Report 90-75, ICAS , 1990.

[27] P.L.Roe. Beyond the Riemann problem I. In , 1992. ICAS - NASA Langley Workshop, September 1991.

[28] P.L.Roe and D.Sidilkover. Optimum positive linear schemes for advection in two and three dimensions. , 29(6):1542–1568, December 1992.

[29] P.L.Roe and L.Beard. An improved wave model for multidimensi

Appendix - A Brief Note on Notation

Due to the complexity of the subject and the huge variety of notation that has been used by a large number of different authors, it seems necessary to include a brief explanation of some of the notation in this report. I have tried to strike a balance between continuing the conventions of previous authors and making this report self-consistent. Unfortunately, few previous papers have presented work on both distribution schemes and wave models and this is reflected here in that there are some inconsistencies in the notation between sections 2 and 3.

The following points should be noted when reading this report.

The sets of flow variables which are used are

_ – conserved variables.

__ – parameter vector variables.

___ – characteristic variables.

_ – primitive variables.

In particular, _ should not be confused in section 3 with , the x-velocity,

_

_